

Near-infrared Image Deblurring and Event Denoising with Synergistic Neuromorphic Imaging

Chao Qu, Shuo Zhu, Yuhang Wang, Zongze Wu, Xiaoyu Chen, Edmund Y. Lam, and Jing Han

Abstract—The fields of imaging in the nighttime dynamic and other extremely dark conditions have seen impressive and transformative advancements in recent years, partly driven by the rise of novel sensing approaches, *e.g.*, near-infrared (NIR) cameras with high sensitivity and event cameras with minimal blur. However, inappropriate exposure ratios of near-infrared cameras make them susceptible to distortion and blur. Event cameras are also highly sensitive to weak signals at night yet prone to interference, often generating substantial noise and significantly degrading observations and analysis. Herein, we develop a new framework for low-light imaging combined with NIR imaging and event-based techniques, named synergistic neuromorphic imaging, which can jointly achieve NIR image deblurring and event denoising. Harnessing cross-modal features of NIR images and visible events via spectral consistency and higher-order interaction, the NIR images and events are simultaneously fused, enhanced, and bootstrapped. Experiments on real and realistically simulated sequences demonstrate the effectiveness of our method and indicate better accuracy and robustness than other methods in practical scenarios. This study gives impetus to enhance both NIR images and events, which paves the way for high-fidelity low-light imaging and neuromorphic reasoning.

Index Terms—Near-infrared imaging, neuromorphic imaging, image deblurring, event denoising.

I. INTRODUCTION

IMAGING in low-light conditions has diverse applications, from micro biomedical analysis to macro astronomy observation, and is especially crucial for ensuring the safety of emerging autonomous driving at night [1, 2]. Under low-light environments, due to limited sensor sensitivity, we have to trade off signal-to-noise ratio for motion blur compensation or vice versa, posing a significant problem for these practical applications. Despite impressive advancements with new hardware and innovative algorithms, enhancing low-light imaging remains a formidable challenge. Near-infrared (NIR) imaging has a unique sensitivity that projects distant objects with clarity, making it particularly useful for night vision applications [3]. NIR imaging has garnered significant attention due to its biomedical imaging, environmental monitoring, and surveillance applications. However, traditional NIR imaging systems often struggle with improper settings, leading to degraded image quality and hindering subsequent analysis with

Chao Qu, Yuhang Wang, Zongze Wu, Xiaoyu Chen, and Jing Han are with Jiangsu Key Laboratory of Spectral Imaging and Intelligent Sense, Nanjing University of Science and Technology, Nanjing 210094, China (e-mail: chao.qu@njust.edu.cn; yhwang@njust.edu.cn; zongze@njust.edu.cn; 115104000466@njust.edu.cn; eohj@njust.edu.cn).

Shuo Zhu and Edmund Y. Lam are with the Department of Electrical and Electronic Engineering, The University of Hong Kong, Pokfulam, Hong Kong SAR, China (e-mail: zhushuo@hku.hk; elam@eee.hku.hk).

Chao Qu and Shuo Zhu contributed equally to this work.

Jing Han and Edmund Y. Lam are the corresponding authors.

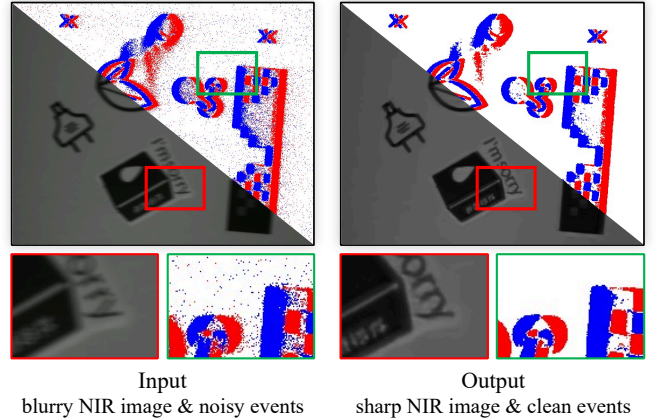


Fig. 1: Comparison examples of shared view with NIR image and events. A single NIR and event camera is often accompanied by motion blur and noise in low-light environments. Our synergistic scheme can reconstruct the sharp NIR image and clean events.

motion blur and artifacts [4]. Additionally, the NIR band exists beyond the human visible spectrum, enabling the use of NIR light that is invisible to humans [5]. Therefore, the NIR images may present structures inconsistent with visible light images, primarily due to the inherent differences in optical properties of the target material across the two spectral regions [6]. Event cameras, capturing visual information as asynchronous events rather than traditional frames, are central to this evolution. This approach mimics the human visual system, enabling superior temporal resolution and improved performance in dynamic scenes. Computational neuromorphic imaging (CNI) with event cameras offers advantages like minimal motion blur and enhanced dynamic range compared to conventional methods. However, the sparse and noisy nature of low-light events leads to a distribution that differs significantly from that in normal light. Events in low-light scenes have distinct distributions prone to various types of interference and increased noise [7, 8]. Although event cameras excel in capturing high-speed motion and low-light conditions, they also present unique challenges, particularly in noise reduction. As shown in Fig. 1, the NIR image suffers from blur, and events are polluted with significant noise in low-light environments. A sharp NIR image and clean events are essential for downstream imaging tasks.

NIR imaging and the CNI paradigm are well characterized, creating a new demand to synergize them for advanced imaging performance. We can surpass these limitations by harness-

ing each attractive property of NIR and event cameras with computational imaging techniques to enhance clarity, detail, and fidelity in NIR images and events. In this work, we focus on fusion consistency and leveraging modal inconsistency, aiming to circumvent its adverse effects on combinations of NIR images and visible events in a new and efficient paradigm. To address the vulnerabilities and limitations of NIR and CNI applications, this paper advocates a novel approach to NIR image deblurring and event denoising by integrating two divergent sensors synergistically.

To address these challenges, the paper contributes by demonstrating:

- We design a synergistic neuromorphic imaging approach for NIR image deblurring and event denoising, leveraging NIR imaging and visible events to enhance performance through complementary strengths.
- We developed a new framework to effectively integrate cross-modal features of NIR images and visible events via spectral consistency and higher-order interaction.
- We build a new cross-spectral deblurring and denoising (CSDD) dataset containing paired NIR images and event streams. Extensive qualitative and quantitative comparisons demonstrate the effectiveness and robustness of the proposed method.

II. RELATED WORK

A. The NIR imaging and Image Deblurring

NIR imaging can capture infrared light at wavelengths between 700 and 1200 nanometers, which is invisible to the human eye. These longer wavelengths exhibit unique scattering and absorption characteristics compared to visible light, allowing NIR imaging to achieve higher signal-to-noise ratios and capture more information, especially in low-light or other challenging environments [9, 10]. As a result, NIR imaging is increasingly applied in computational imaging and computer vision, showing great potential in applications such as image denoising [11, 6], image fusion [5, 12], material classification [13], and scene category recognition [14]. However, NIR cameras often have low frame rates, leading to motion blur. Traditional deblurring methods, which rely on deconvolution algorithms [15, 16] or specific priors [17, 18], face limitations in generalization and effectiveness. Recently, deep learning approaches have shown improvements in image reconstruction quality by learning the complex mapping between blurry and sharp images [19, 20, 21, 22, 23, 24]. Additionally, some works have applied the high temporal resolution of event cameras to image deblurring, achieving better results than traditional frame-based methods [25, 26, 27, 28, 29, 30, 31, 32]. Unlike these approaches, this paper focuses on the collaborative enhancement of NIR and event cameras, aiming to achieve NIR images deblurring through cross-spectral information fusion.

B. The CNI paradigm and Event Denoising

Unlike conventional cameras that capture full images at a fixed rate determined by an external clock, event cameras are

retinomorphic devices that trigger an event once the observed logarithmic intensity variation exceeds a preset threshold and record the fast dynamics more effectively [7]. This makes them ideally suited for advanced sensing and offers significant potential for computer vision and computational imaging in challenging scenarios [33, 8]. The high sensitivity with logarithmic response raises exciting possibilities for low-light imaging, offering superior performance to scientific detectors and enabling high-resolution imaging ability and weak signal detection [34]. However, event cameras with logarithmic response are particularly susceptible to different types of interference, leading to increased noise levels. Therefore, denoising of events becomes a crucial preprocessing step for downstream tasks [35, 36]. Research on event denoising is primarily categorized into filtering-based methods and learning methods. Filtering-based methods rely on manual priors to design discriminative models for noise removal, employing techniques like density distinction with motion continuity [37, 38], and motion compensation within the spatiotemporal domain [39]. However, the effectiveness of these priors can vary with different signal/noise event distributions, which may limit their denoising accuracy. Learning-based methods for event denoising have been studied and used recently, such as EDnCNN [40], EventZoom [41], AEDNet [42], LED [43], etc. Given the growing need for sensitive and dynamic processing capabilities, CNI-informed techniques that provide high-quality events with reduced noise are essential for driving progress in complex applications.

III. METHODOLOGY

A. Problem Formulation

We first revisit the fundamental models for motion deblurring and event denoising. Next, we establish a unified task framework that is based on NIR and neuromorphic imaging, to integrate the complementary advantages of synergistic imaging and simultaneously achieve NIR motion deblurring and event denoising. For this unified task, we propose a dual-modal synergistic scheme in the following section.

Motion Deblurring. The blurry NIR image B , can be formulated as the average of the latent intensity images $I(t)$ over the exposure interval T

$$B = \frac{1}{T} \int_0^T I(t) dt, \quad (1)$$

where T denotes the exposure time. The motion deblurring aims at recovering a sharp NIR image S from the blurred image B

$$S = \mathcal{B}^{-1}(B, E), \quad (2)$$

where \mathcal{B}^{-1} represents the NIR motion deblurring operation assisted by the event streams $E = \{(x_i, y_i, t_i, p_i)\}_{i=0}^T$. Here, x_i and y_i indicate the pixel positions, t_i represents the time of the i -th event, and $p_i \in \{-1, +1\}$ denotes polarity, representing brightness change directions.

Event Denoising. Due to hardware limitations, events are inevitably contaminated by noise N , especially in low-light

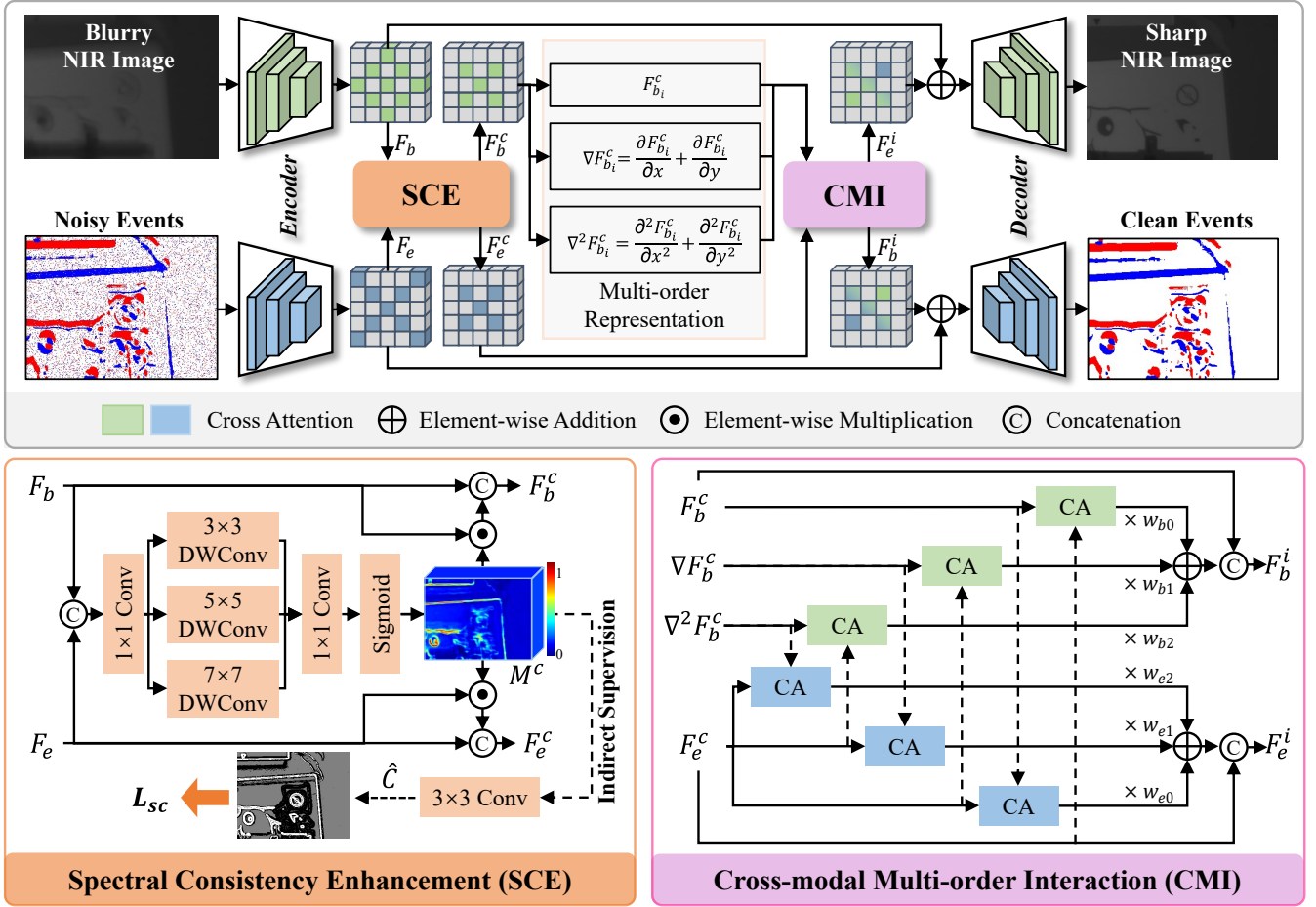


Fig. 2: Architecture of the proposed MDEDNet, which consists of a dual-branch subnetwork, a spectral consistency enhancement (SCE) module, and a cross-modal multi-order interaction (CMI) module. MDEDNet takes a blurry NIR image and noisy events as input, and through collaborative enhancement, simultaneously outputs a sharp image and clean events.

conditions

$$E_n = E_c + N, \quad (3)$$

where E_c represents the noise-free events, and E_n is the noisy events. The goal of event denoising is to recover the noise-free event E_c from the noisy event E_n

$$E_c = \mathcal{E}^{-1}(E_n, I), \quad (4)$$

where \mathcal{E}^{-1} denotes the event denoising operation assisted by NIR images I .

Unified Task. The unified task is simultaneous NIR image deblurring and event denoising, which can be expressed as

$$S, E_c = \mathcal{B}\mathcal{E}^{-1}(B, E_n), \quad (5)$$

where $\mathcal{B}\mathcal{E}^{-1}$ represents a unified NIR motion deblurring and event denoising operation based on synergistic neuromorphic imaging.

B. Synergistic Scheme

We propose a novel NIR and event cooperative enhancement network, MDEDNet, which simultaneously achieves image motion deblurring and event denoising by exploring the mutual compensation between degraded dual-modal (blurred NIR

images and noisy events). Fig. 2 illustrates the architecture of the proposed MDEDNet, which consists of a dual-branch subnetwork, a spectral consistency enhancement (SCE) module, and a cross-modal multi-order interaction (CMI) module. Each branch of the subnetwork adopts a multi-scale encoder-decoder structure, with encoding and decoding layers at each scale consisting of two Res Blocks.

1) *Spectral Consistency Enhancement:* Since NIR imaging and event imaging capture information in different spectral bands (*i.e.*, NIR and visible wavelength), structural discrepancies may occur between the events and NIR images in certain scenes. Ignoring this structural inconsistency during the fusion of these heterogeneous data may introduce artifacts, thereby reducing the accuracy of dual-modal cooperative enhancement. To address this issue, we propose a Spectral Consistency Enhancement (SCE) module, which assigns pixel-level weights by predicting a spectral consistency map M^c to suppress inconsistent structures between NIR and event features.

As illustrated in Fig. 2, the NIR feature $F_b \in \mathbb{R}^{C \times H \times W}$ and event feature $F_e \in \mathbb{R}^{C \times H \times W}$ are used as inputs to estimate the spectral consistency map $M^c \in \mathbb{R}^{C \times H \times W}$. Then, M^c is multiplied with F_b and F_e respectively to enhance common

features. This process is described as follows

$$\begin{aligned} M^c &= \text{SCE}(F_b, F_e), \\ F_b^c &= \text{Concat}([F_b, F_b \odot M^c]), \\ F_e^c &= \text{Concat}([F_e, F_e \odot M^c]), \end{aligned} \quad (6)$$

where \odot denotes the element-wise multiplication operation. F_b^c represent the NIR consistency enhancement features. F_e^c represent the event consistency enhancement features. To improve the estimation accuracy of the spectral consistency map M^c , we use large-kernel depth-wise convolutional layers [44] to capture richer structural information. Specifically, we integrate depth-wise convolutional layers with various kernel sizes (*i.e.*, 3×3 , 5×5 , 7×7) in the SCE and then use a 1×1 convolution to aggregate features under different receptive fields. Finally, the aggregated features are nonlinearly mapped to the spectral consistency map M^c through the Sigmoid function according to the relative importance of each pixel location.

Considering SCE struggles to naturally capture structural differences in the feature dimensions between NIR images and events, we introduce explicit supervision to the SCE for generating a high-accuracy M^c . Inspired by [9], we calculate the structure consistency $C \in \mathbb{R}^{1 \times H \times W}$ between the visible image corresponding to the events and the NIR image. The definition for C is as follows

$$C = \frac{1}{2}(1 - S^v)(1 - S^n) + S^v \times S^n, \quad (7)$$

where S^v denotes the edges of the visible image and S^n denotes the edges of the NIR image. The pixel value of C varies from 0 to 1, with 0 indicating inconsistent structure and 1 indicating consistent structure, which is suitable for the supervision of SCE. Considering the dimensional difference between C and M^c , we decode the potential structure consistency $\hat{C} \in \mathbb{R}^{1 \times H \times W}$ from the high-dimensional M^c by a 3×3 convolution and constrain it through a spectral consistency loss L_{sc} , which can be expressed as

$$L_{sc} = |C - \hat{C}|_2 = |C - \text{Conv}(M^c)|_2. \quad (8)$$

This approach can indirectly provide effective supervision for the high-dimensional feature space of NIR and events, guiding the SCE module to generate a physically meaningful spectral consistency map M^c , providing reliable and accurate spatiotemporal features for subsequent cross-modal multi-order interaction.

2) *Cross-modal Multi-order Interaction*: The significant differences in sparsity and signal-to-noise ratio exist between NIR images and events. Previous studies have not thoroughly investigated the relationships between these two modalities and typically apply concatenates [45] or basic attention mechanisms [27] to fuse the two modal features. Such interaction methods often struggle to achieve satisfactory results when dealing with complex scenarios.

To comprehensively analyze the correlation between events and the NIR image, we visualize the events, NIR image, multi-level gradient signals of the image, and their corresponding histograms. First, both the event and image gradient signals reveal the texture features of the scene. As illustrated in Fig.

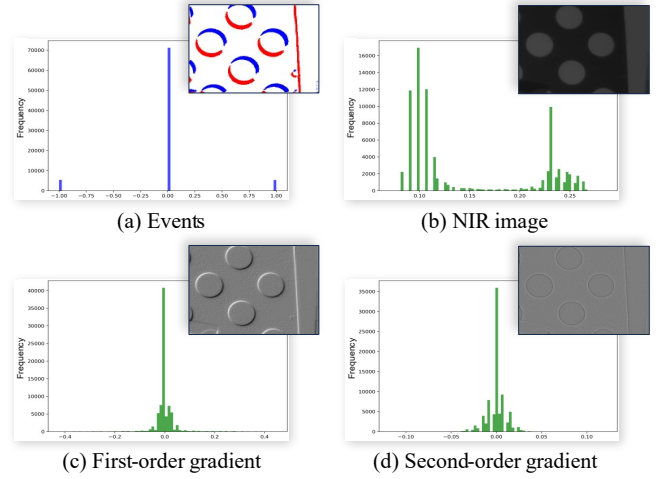


Fig. 3: (a)-(d) represent events, NIR image, first-order and second-order gradient, respectively, along with their histograms.

3, the event camera captures brightness changes in the scene, making edges more likely to trigger events, while flat regions have a lower probability of triggering events. Image gradients can precisely capture the texture details in the image, and these texture features exhibit a spatial distribution similarity with the events. Furthermore, both the event signals and image gradient signals exhibit significant sparsity. The histogram in Fig. 3 shows that most pixels in the original image signal have non-zero values, while the most pixels in the image gradients and events are zero. This sparsity indicates that the multi-order gradient signals of sharp images and the event information have substantial collaborative potential in modal interaction.

Based on the above analysis, we propose a cross-modal multi-order interaction (**CMI**) module that achieves fine-grained fusion between dual modalities through interaction between event features and multi-order image gradients. Specifically, the first-order gradient effectively captures large-scale structural details, helping to identify prominent edges in the scene [46]. The second-order gradient, by capturing higher-order edge information at smaller scales, enables more sensitive recognition of subtle texture variations [12]. We therefore integrate image features, first-order gradients, and second-order gradients to mitigate the limitations of a single gradient.

As illustrated in Fig. 2, in the feature interaction from events to images, we first compute the first- and second-order gradients of the consistency image features F_b^c . Next, we generate the Q_{b0} , Q_{b1} , and Q_{b2} matrices from the multi-order gradient features, while generating the corresponding K_e and V_e matrices from the consistency event features F_e^c . We then perform lookups of event features using multi-order gradient features, followed by weighted summation for fusion. Finally, we concatenate the fused features with the event features to obtain the interaction features F_e^i . This process can be

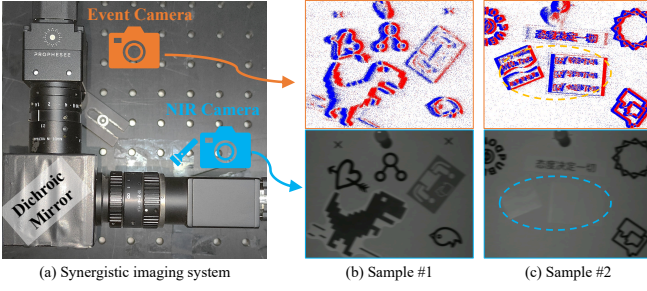


Fig. 4: (a) The synergistic imaging system with a NIR camera and an event camera. (b) and (c) Two imaging samples with raw collected NIR images and corresponding noisy events. Notably, the dashed line area in sample #2 highlights spectral inconsistencies between the NIR and the events.

represented as:

$$\begin{aligned} F_{e0} &= CA(Q_{b0}, K_e, V_e) \\ F_{e1} &= CA(Q_{b1}, K_e, V_e) \\ F_{e2} &= CA(Q_{b2}, K_e, V_e) \end{aligned} \quad (9)$$

$$F_e^i = \text{Concat}([F_e^c, (w_{e0} * F_{e0} + w_{e1} * F_{e1} + w_{e2} * F_{e2})]),$$

where $CA(\cdot)$ denotes the cross attention operation [47], F_{ej} represents the queried event features corresponding to the j -th order gradient, and w_{ej} is the learnable weight for the j -th order gradient. The process of information interaction from events to images mirrors that from images to events.

By integrating the multi-order features of the image with the spatiotemporal features of the event, we achieve a deep-level interaction between different modalities, effectively reducing image blur and minimizing event noise.

3) *Loss Function*: The motion deblurring task is supervised by the $l1$ norm between a predicted sharp image \hat{S} and the ground truth sharp image S , as follows

$$L_{md} = \|\hat{S} - S\|_1. \quad (10)$$

The event denoising task is supervised by the $l2$ norm between the predicted event \hat{E}_c and the ground truth clean event E_c , which can be defined as

$$L_{ed} = \|\hat{E}_c - E_c\|_2. \quad (11)$$

Thus, the total loss function for MDEDNet is defined as

$$L_{total} = \lambda_1 L_{md} + \lambda_2 L_{ed} + \lambda_3 L_{sc}, \quad (12)$$

where λ_1 , λ_2 and λ_3 represent the weights of each loss.

IV. CSDD DATASET

To our knowledge, there is currently no publicly available dataset for NIR and event camera cooperative tasks. This prompted us to establish a new dataset for cross-spectral deblurring and denoising (CSDD), which includes paired blurry-sharp NIR images and corresponding noisy event streams.

To simultaneously capture NIR images and events, we built a synergistic imaging system with an event camera (Prophesee EVK5, 1280×720) and a NIR camera (HIKROBOT MV-CA016-10GM, 1440×1080), as shown in Fig. 4. To ensure minimum spatial parallax between the NIR camera and the

event camera, a dichroic mirror with a cutoff wavelength of 805nm is used to separate the visible light and NIR information reflected from the target. Additionally, an 850 nm NIR illuminator is provided for the NIR camera.

We collect 45 sequences comprising NIR image sequences and event streams, covering various illumination conditions and spectral response scenarios. During data acquisition, we fix the target object on a motorized rail to achieve precise motion control, enabling the imaging system to capture NIR sequences and event streams simultaneously. To obtain event streams with different noise levels, we conduct imaging under both normal and low-light conditions. Furthermore, we take the impact of spectral inconsistency and select target scenes with different visible light and NIR spectral responses. Since the two cameras provide different visual modalities, calibration in both spatial and temporal domains is crucial to ensure alignment between the collected NIR images and event data. Similar to previous work [28], we adopt an approximate temporal synchronization strategy, writing a script to simultaneously trigger the capturing programs of the two cameras. We then estimate the homography matrix between the two cameras by manually selecting feature points, achieving geometric alignment of the NIR image sequences with the event stream. In our experiments, we crop the central region of both NIR images and event streams to 640×512 pixels.

V. EXPERIMENTS

A. Implementation Details and Metrics

We create a synthetic dataset based on the visible-nir dataset DVD [9] for network training and evaluation. Specifically, we first generate visible and NIR image sequences according to previous work [28], and then construct blurry-sharp pairs of NIR images. Additionally, we use the open-source event simulator (ESIM) [48] to generate event streams corresponding to the visible images, and we create paired noise-clean event streams by introducing noise. We convert the event stream into a voxel grid representation and set the bin size of event voxels to 13. Furthermore, we use captured CSDD datasets to verify the performance of the proposed method in real-world scenarios.

We set the batch size to 16 and train for 200 epochs. We utilize the Adam optimizer [49] with an initial learning rate of 0.0005. The learning rate remains unchanged for the first 100 epochs and gradually decreases to 0 over the next 100 epochs. Patches at the size of 128×128 are randomly cropped from training samples, and random horizontal or vertical flips are applied. All experiments were conducted on a server using Python 3.8.0, PyTorch 1.12.0, and NVIDIA GeForce RTX 3090. The weighting factors λ_1 , λ_2 , and λ_3 in Eq. 12 are set to 1, 1, and 0.1, respectively. We use structural similarity (SSIM) and peak signal-to-noise ratio (PSNR) as performance metrics for motion deblurring and use root mean square error (RMSE) as performance metrics for event denoising [50].

B. Comparison of Motion Deblurring

We first evaluate the performance of our MDEDNet on the motion deblurring task. Both qualitative and quantitative

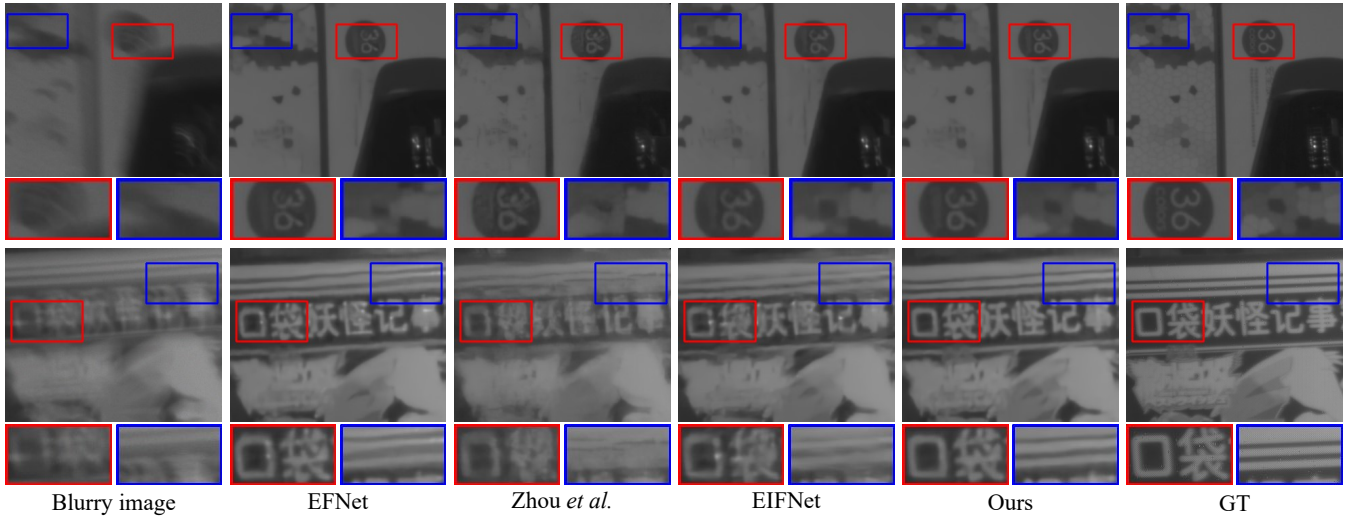


Fig. 5: Comparison results of our deblurring method with others on the synthetic dataset.

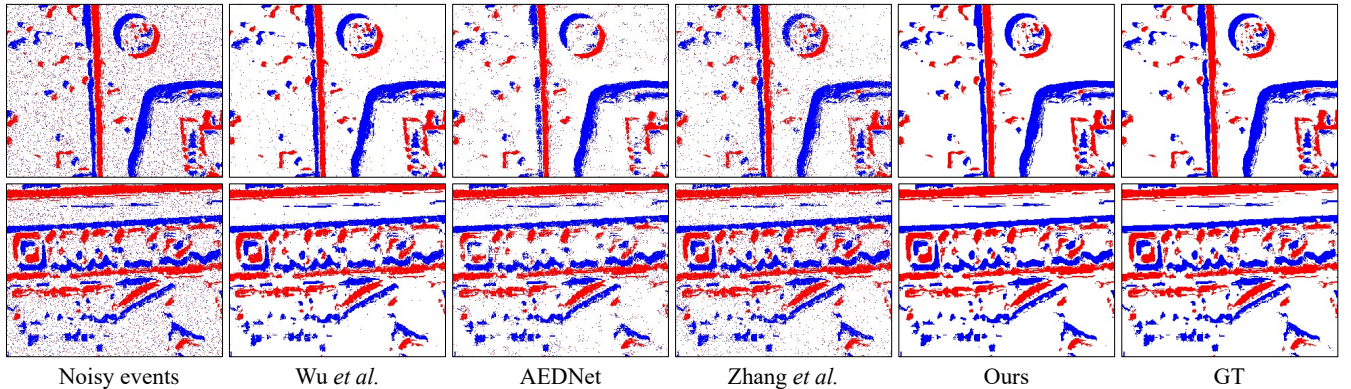


Fig. 6: Comparison results of our denoising method with others on the synthetic dataset.

TABLE I: Quantitative comparisons of the proposed MD-EDNet to the state-of-the-art motion deblurring methods on the synthetic and CSDD datasets. The best performance is in bold.

Method	Event	Params (M)	Synthetic		CSDD	
			PSNR	SSIM	PSNR	SSIM
LEDNet [20]	✗	7.4	34.07	0.8526	27.58	0.8686
DeepRFT [22]	✗	9.6	35.67	0.9074	28.23	0.8753
FSNet [51]	✗	14.8	35.35	0.9040	26.04	0.8388
MISCFilter [24]	✗	17.1	35.45	0.9053	28.38	0.8821
EFNet [27]	✓	8.5	36.90	0.9134	34.64	0.9531
Zhou <i>et al.</i> [28]	✓	11.8	34.88	0.8955	32.99	0.9313
EIFNet [30]	✓	10.8	36.97	0.9227	34.89	0.9551
Ours	✓	4.8	37.79	0.9248	35.80	0.9618

comparisons are made with state-of-the-art frame-based methods, including LEDNet [20], DeepRFT [22], FSNet [51], and MISCFilter [24], as well as event-based methods, including EFNet [27], Zhou *et al.* [28], and EIFNet [30]. Their official code is used and retrained to achieve optimal performance. Table I shows that our method outperforms other methods in deblurring both synthetic and CSDD datasets. Specifically, on

TABLE II: Quantitative comparisons of the proposed MD-EDNet to the state-of-the-art event denoising methods on synthetic dataset. The best performance is in bold.

	Wu <i>et al.</i> [52]	AEDNet [42]	Zhang <i>et al.</i> [50]	Ours
RMSE	0.1896	0.2042	0.1977	0.1159

the synthetic dataset, our method improves performance by 2.12 dB over the best frame-based methods and by 0.82 dB over the best event-based methods. Additionally, Figs. 5 and 7 present qualitative visual comparisons on synthetic and CSDD datasets, respectively. Overall, these visual comparisons indicate that our method can recover sharper texture details and demonstrate strong generalization performance on real scenes.

C. Comparison of Event Denoising

Furthermore, we compare MD-EDNet with state-of-the-art event denoising methods, including Wu *et al.* [52], AEDNet [42], and Zhang *et al.* [50]. Table II shows that the proposed method achieves the lowest RMSE on the synthetic dataset. Figs. 6 and 8 illustrate the qualitative results on the synthetic and CSDD datasets. The results indicate that, compared to

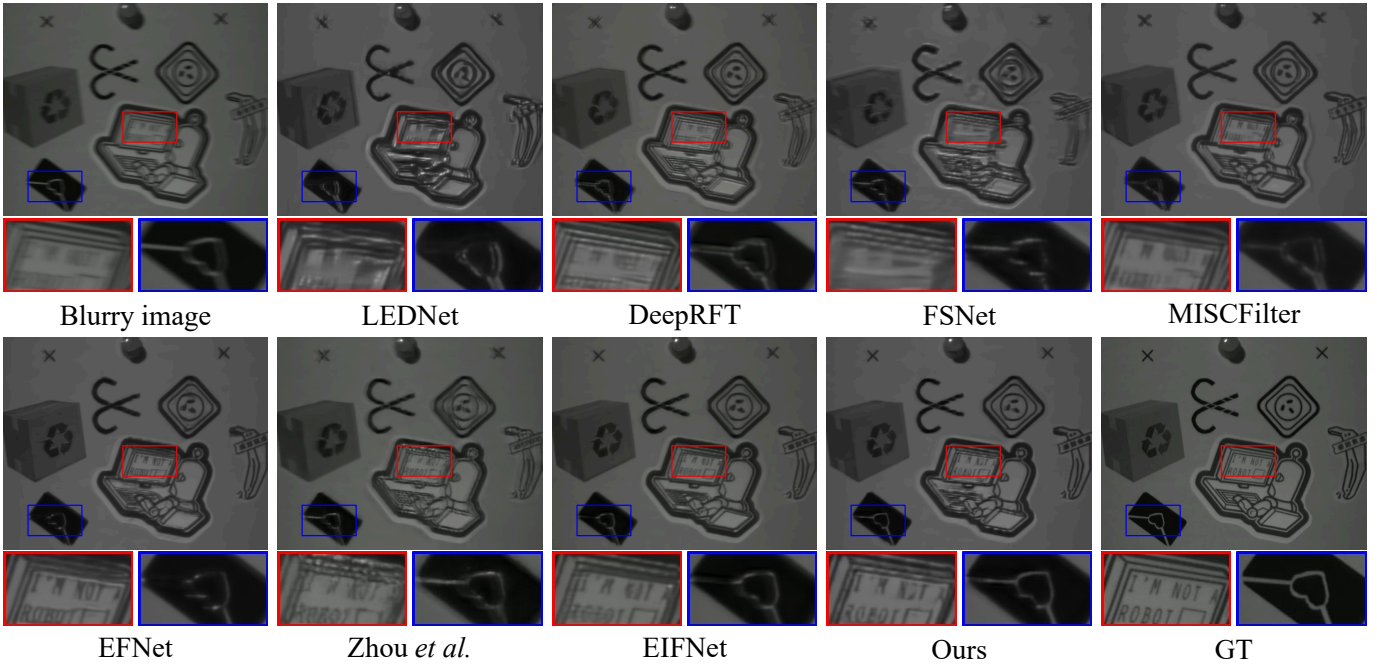


Fig. 7: Comparison results of our deblurring method with others on the CSDD dataset.

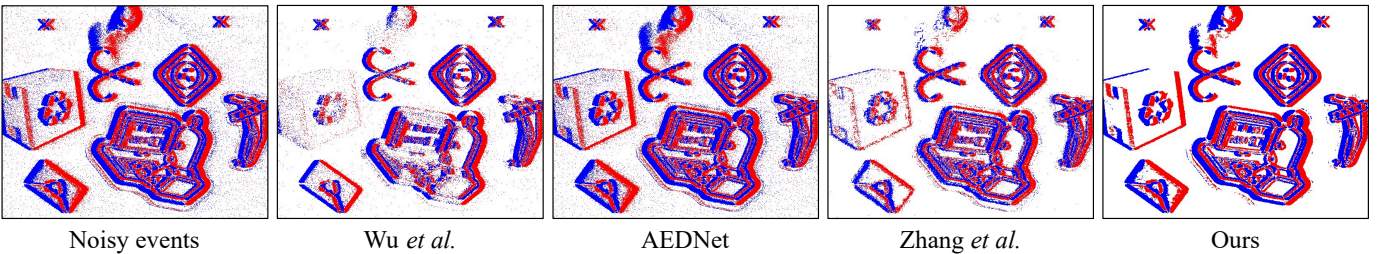


Fig. 8: Comparison results of our denoising method with others on the CSDD dataset.

TABLE III: Ablation study of SCE and CMI modules on the synthetic dataset. CMI_j represents the cross-modal interaction based on the j -th order gradient. The best performance is in bold.

Case	SCE	CMI_0	CMI_1	CMI_2	PSNR	SSIM	RMSE
#1					36.77	0.9139	0.1188
#2	✓				37.20	0.9188	0.1185
#3	✓	✓			37.62	0.9217	0.1171
#4	✓	✓	✓		37.73	0.9230	0.1164
#5	✓	✓	✓	✓	37.79	0.9248	0.1159

other state-of-the-art methods, the proposed method demonstrates a significant advantage in event denoising performance.

D. Ablation Study

SCE Module. The SCE module allocates pixel-level weights by predicting the spectral consistency map M^c . As shown in Table III, the introduction of the SCE module increases the PSNR of MDEDNet by 0.43 dB. This result highlights the significant role of the SCE module in improving the deblurring performance. Furthermore, Fig. 9 shows the spectral response and the spectral consistency map M^c generated by the SCE

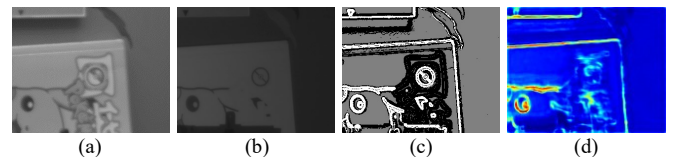


Fig. 9: (a) and (b) are the visible light and NIR responses of the same scene. (c) The structural consistency C between different spectral responses. (d) The predicted spectral consistency feature map M^c .

module. The visualization results show that the SCE module effectively identifies inconsistent structures in the scene, thereby significantly enhancing the common features in both NIR and event data.

CMI Module. The CMI module aims to achieve deep fusion between NIR and event features. As shown in Table III, the PSNR of MDEDNet decreases by 0.59 dB without the CMI module. This result indicates that the CMI module plays a significant role in the collaborative enhancement of the two modalities. Furthermore, we analyze the contribution of different gradient information to cross-modal interaction. As shown in Table III, introducing first-order and second-order gradients effectively improves the deblurring and denoising performance of MDEDNet.

TABLE IV: Ablation study of loss functions on the synthetic dataset. The best performance is in bold.

Case	L_{md}	L_{ed}	L_{sc}	PSNR	SSIM	RMSE
#1	✓			37.35	0.9206	—
#2		✓		—	—	0.1403
#3	✓	✓		37.59	0.9228	0.1261
#4	✓	✓	✓	37.79	0.9248	0.1159

Loss Functions. For the motion deblurring task, it is observed from Table IV that removing L_{ed} and L_{sc} leads to a degradation in reconstruction results. This is because L_{ed} introduces high-quality event streams, providing valuable spatiotemporal references for NIR deblurring. For the event denoising task, removing L_{md} and L_{sc} results in a decrease in denoising metrics, indicating that L_{md} and L_{sc} contribute to recovering noise-free events. L_{sc} effectively constrains spectral consistency, enabling highly relevant features for interactions between the NIR and event data.

VI. CONCLUSION

In conclusion, this paper introduced a novel framework to address motion blur in NIR imaging and severe noise in neuromorphic imaging under low-light conditions. To tackle these issues, we developed a synergistic neuromorphic imaging framework for jointly achieving NIR image deblurring and event denoising. Empirical evidence demonstrates that our spectral consistency enhancement significantly promotes cross-modal interaction and enhances imaging performance. This design effectively mitigates the gap caused by cross-modal differences and improves imaging capability in extremely dark scenes. Furthermore, to evaluate the synergistic neuromorphic imaging method, this study collected the NIR and event stream dataset, specifically tailored for low-light environments and varying system settings, further underscores our contribution by providing a robust platform for testing and benchmarking low-light NIR and event-based algorithms. Our scheme provides an enlightening reference for cross-modal tasks, highlighting its potential for challenging applications.

VII. SUPPLEMENTARY MATERIAL

In the supplementary material, we provide additional experimentation details, further analysis of spectrum and spectral consistency enhancement (SCE), further ablation experiments on cross-modal multi-order interaction (CMI), and additional qualitative results.

We further provide a supplementary video to show our experimental platform, cross-spectral deblurring and denoising (CSDD) dataset, and results for both synthetic and real-world scenes.

A. Additional Experimentation Details

1) *Network Architecture:* To achieve joint optimization for NIR motion deblurring and event denoising, we design a dual-branch subnetwork. Each branch adopts a multi-scale encoder-

decoder structure. The encoder comprises three encoding layers, with each layer containing two Res Blocks. The encoding process can be represented as

$$F_b = \mathcal{E}_b(B), \quad F_e = \mathcal{E}_e(E_n), \quad (13)$$

where B and E_n represent blurry NIR image and noisy events respectively. \mathcal{E}_b and \mathcal{E}_e denote the image encoder and event encoder, respectively. F_b and F_e represent the encoded features of image and event. Unlike single-task approaches, the proposed cooperative task requires fully leveraging the complementary advantages of both modalities. Therefore, we perform an efficient interactive fusion of the NIR-encoded and event-encoded features. The fusion process can be expressed as

$$F_b^i, F_e^i = \text{CMI}(\text{SCE}(F_b, F_e)), \quad (14)$$

where F_b^i and F_e^i represent the image interaction features and event interaction features, respectively. SCE denotes the spectral consistency enhancement module, and CMI signifies cross-modal multi-order interaction. The interaction features are then passed to the decoder, generating sharp images and clean events respectively. The structure of the decoder is similar to that of the encoder. The decoding process can be represented as

$$\hat{S} = \mathcal{D}_b(F_b + F_e^i), \quad \hat{E}_c = \mathcal{D}_e(F_e + F_b^i), \quad (15)$$

where \mathcal{D}_b and \mathcal{D}_e denote the image decoder and event decoder, respectively. \hat{S} and \hat{E}_c represent predicted sharp NIR image and clean events respectively.

2) *Synthetic Dataset Generation Pipeline:* The generation process of the synthetic dataset generally follows the method described in [28], with necessary adjustments and optimizations based on the unified tasks of NIR deblurring and event denoising. The Dark Vision Dataset [9] is chosen as the ideal data source for constructing this synthetic dataset due to its inclusion of noise-free, paired visible light and NIR images. Specifically, for each scene, the synthetic dataset generation process can be described by the following steps:

- Randomly crop the source image to 320×256 pixels to obtain a sharp NIR image S and its corresponding visible light image;
- First, the Sobel filter is applied to both the visible light and NIR images for edge detection. Then, edge binarization is performed to calculate the structural consistency C ;
- The camera motion trajectory is randomly generated using the algorithm proposed in [53];
- The visible light and NIR images are moved along pixel-level trajectories, resulting in an image sequence containing multiple potential frames during the exposure period;
- The event simulator (ESIM) [48] is used to generate the corresponding noise-free events E_c from the visible light image sequence. Simultaneously, the NIR image sequence undergoes averaging to produce the blurry NIR image B ;
- Noise is added to the noise-free event E_c according to the

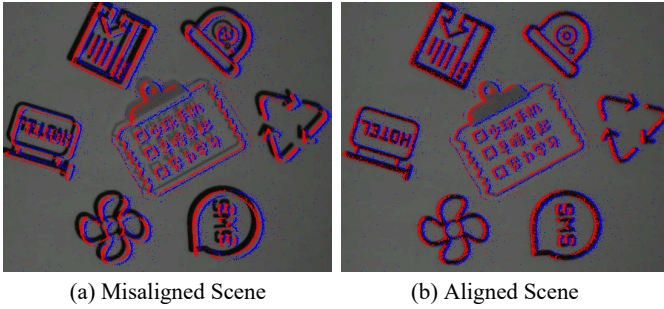


Fig. 10: Alignment of NIR image with events. Aggregated events (red is positive, and blue is negative) are overlain with the NIR image.

Poisson process to generate noisy events E_n , and noise is also added to the blurry NIR image B to make it more representative of actual observations in real-world scenes [54].

For each scene, we randomly generate 20 different camera motion trajectories. The final training dataset contains 4000 different images, and the test dataset contains 600 different images.

3) *CSDD Dataset Calibration*: Similar to previous work [28], we adopt an approximate temporal synchronization strategy, writing a script to simultaneously trigger the capturing programs of the two cameras. We then estimate the homography matrix between the two cameras by manually selecting feature points, achieving geometric alignment of the NIR image sequences with the event stream. Fig. 10 illustrates a typical example of the calibration results.

B. Further Analysis on Spectrum and SCE

NIR and visible light primarily rely on the reflective properties of objects for information acquisition and analysis, which sharply contrasts with the working principle of long-wave infrared, based on the emissive properties of objects [4]. Specifically, NIR and visible light exhibit significant similarities in many aspects, primarily due to their relative proximity in the spectral range and shared adherence to the physical mechanisms of reflection. However, despite these commonalities, the differences in wavelength range and the inherent variations in material reflectance can lead to inconsistent response characteristics of NIR and visible light under certain application scenarios. Therefore, when utilizing NIR cameras and event cameras for synergistic enhancement, it is necessary to thoroughly consider and distinguish their unique response characteristics.

The SCE module predicts and generates a spectral consistency map M^c by assessing the similarities and differences between NIR responses and event responses within a scene. The M^c assigns corresponding weight values to each pixel based on distinct structural features. As shown in the blue box area of Fig. 11, regions with consistent spectral responses receive higher weights, whereas those with inconsistent responses are assigned lower weights.

To further evaluate the influence of the SCE module on deblurring performance, we set all values in the M^c to zero,

TABLE V: Quantitative comparisons of different fusion methods on the synthetic dataset. CMI_j represents the cross-modal interaction based on the j -th order gradient. The best performance is in bold.

Fusion	Add	Concat.	Attention	CMI_0	$CMI_{0,1}$	$CMI_{0,1,2}$
PSNR	36.77	36.44	37.12	37.17	37.28	37.39
SSIM	0.9139	0.9136	0.9143	0.9145	0.9177	0.9193

producing the corresponding deblurred image S_0 . A M_0^c with all-zero values cannot provide pixel-level guidance for the fusion of NIR and event features, leading to undesired artifacts in S_0 . In contrast, the M^c predicted by the SCE module accurately reflects the response differences between NIR and visible light in the scene. The deblurred image S demonstrates that the SCE module facilitates the recovery of sharp edges.

In addition, in certain application scenarios, it may be necessary to simultaneously integrate NIR and event information to achieve comprehensive reconstruction of both consistent and inconsistent regions. The SCE module effectively identifies differences in spectral responses within the scene, enabling subsequent fusion processes to adapt based on the M^c . This adaptability implies that manually modifying the values of the M^c enables diverse reconstruction results. For instance, setting all values in the M^c to 1 signifies that both NIR and event responses are fully incorporated into the fusion. As illustrated in the red box area of Fig. 11, the deblurred image S_1 effectively integrates information that is originally absent in the NIR, thereby improving both the reconstruction quality and the richness of details.

C. Further Ablation Experiments on CMI

To further validate the effectiveness of the CMI module, we compare it with several common fusion methods, including addition, concatenation, and cross-attention. As shown in Table V, fusing complementary information from two modalities through simple addition or concatenation has limited effectiveness, making it difficult to fully leverage the synergy between modalities. Although the cross-attention captures the relevant parts of features from both modalities, relying solely on shallow interactions between the image and event domains is insufficient to achieve optimal results. In contrast, CMI significantly enhances deblurring performance by fine-grained fusion of multi-order gradient features from images with event features, demonstrating its superiority in capturing cross-modal information.

D. Additional Qualitative Results

1) *Low-light Environment*: Fig. 12 illustrates qualitative results of NIR deblurring and event denoising in low-light environment. Under an illumination condition of 0.5 lux, visible light image fail to convey clear scene information. Although contrast stretching enhances the visual clarity of the image, it simultaneously introduces significant noise. Event cameras, though highly sensitive in low-light environments, are prone to capturing substantial noise in their event data.

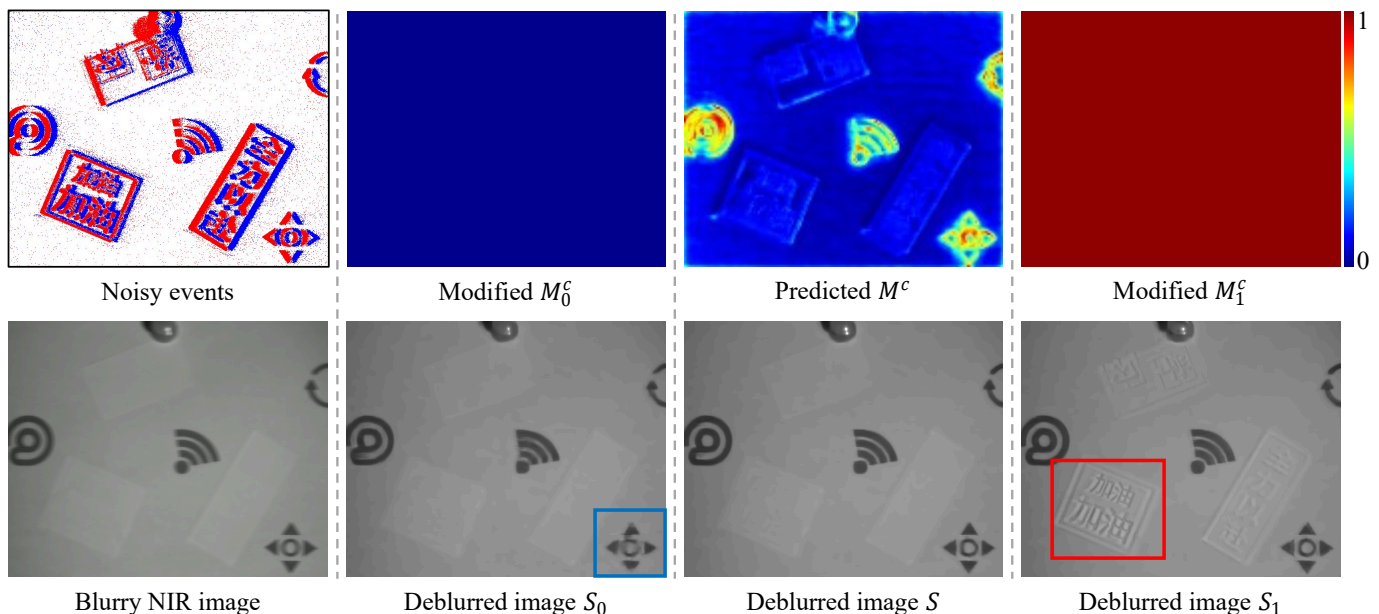


Fig. 11: Deblurred results corresponding to M^c with different values. The SCE module can effectively identify consistent structures in the scene and generate the spectral consistency map M^c . When M^c is set to 0, unexpected artifacts appear in the deblurred image S_0 . When M^c is set to 1, the deblurred image S_1 effectively integrates information that was not originally present in the NIR image.

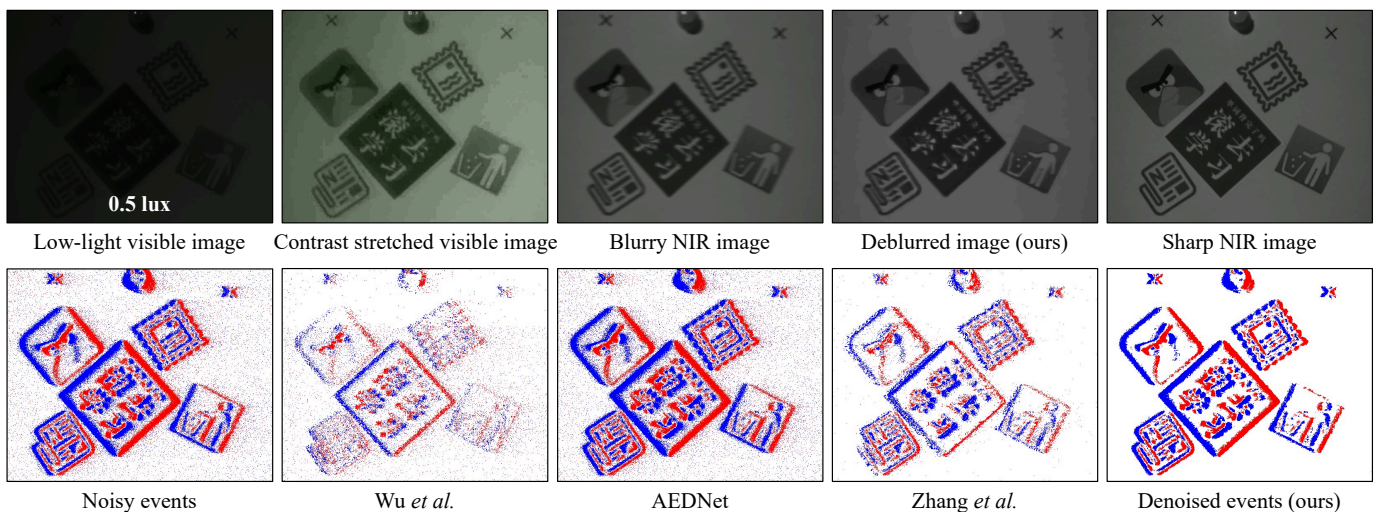


Fig. 12: Comparison of visible light image, events, and NIR image in low-light environment, as well as the NIR deblurring and event denoising results of the proposed method. Our method effectively reconstructs sharp NIR image and clean events in challenging environment.

In contrast, NIR image achieves a higher signal-to-noise ratio under such conditions but is susceptible to motion blur in dynamic scenes. In the unified task of NIR motion deblurring and event denoising, NIR cameras and event cameras demonstrate significant complementary advantages. Experimental results demonstrate that the proposed method effectively reconstructs sharp NIR image and high-quality, clean events in challenging environment.

2) *Synthetic Dataset*: Figs. 13 and 14 provide additional qualitative results for NIR deblurring and event denoising on the synthetic dataset, respectively. In the image deblurring task, frame-based deblurring methods face significant

challenges when reconstructing sharp images directly from blurry ones in complex dynamic scenes. Although event-based deblurring methods show improvements in reconstruction quality, their results are often accompanied by artifacts and distortions due to event noise and spectral inconsistencies. In contrast, the proposed method effectively improves deblurring quality by introducing a spectral consistency enhancement module and a cross-modal multi-order interaction module. For the event denoising task, aided by high signal-to-noise ratio NIR images, the proposed method effectively suppresses event noise.

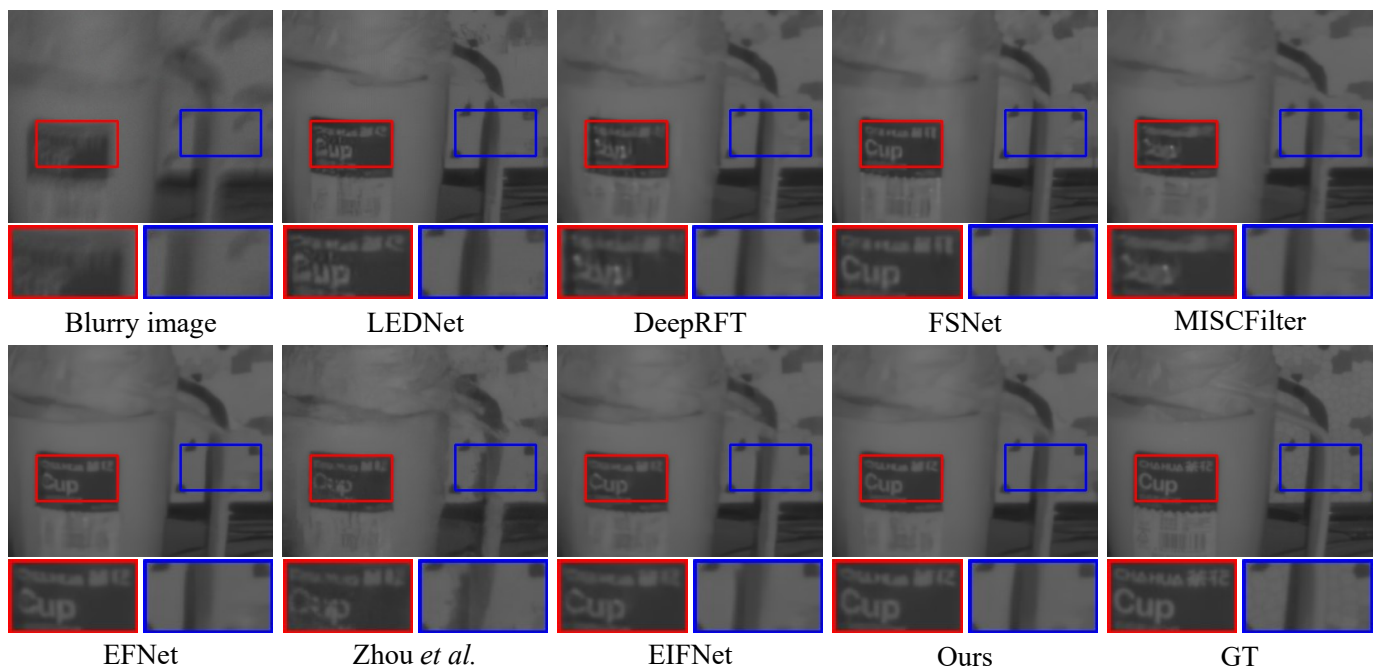


Fig. 13: Comparison results of our deblurring method with others on the synthetic dataset.

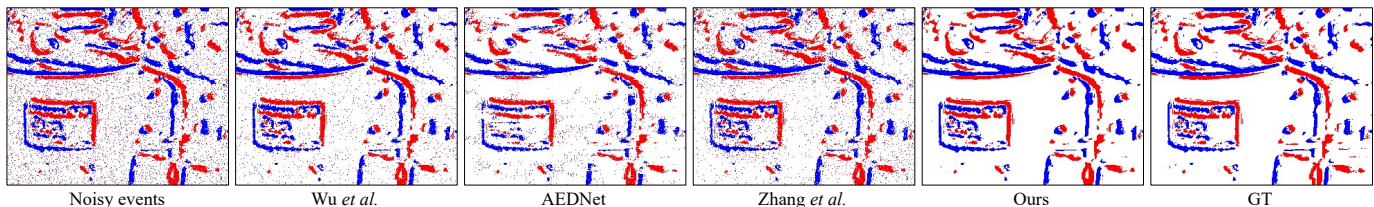


Fig. 14: Comparison results of our denoising method with others on the synthetic dataset. The events come from the same scene as the NIR in Fig. 13.

3) *CSDD Dataset*: Figs. 15 and 17 present additional qualitative results of NIR deblurring on the CSDD dataset, while Figs. 16 and 18 provide additional qualitative results of event denoising on the same dataset. Figs. 15 and 16, as well as Figs. 17 and 18, correspond to the same scenes with NIR responses and event responses, respectively. Specifically, Figs. 15 and 16 do not contain spectrally inconsistent structures, whereas Figs. 17 and 18 include spectrally inconsistent structures. These results demonstrate that, regardless of whether spectral inconsistency is present in the scene, the proposed method reconstructs sharp images from blurred NIR inputs and restores clean events from noisy ones. Compared with contrasting methods, the proposed method shows significant advantages in deblurring and denoising performance in real scenes.

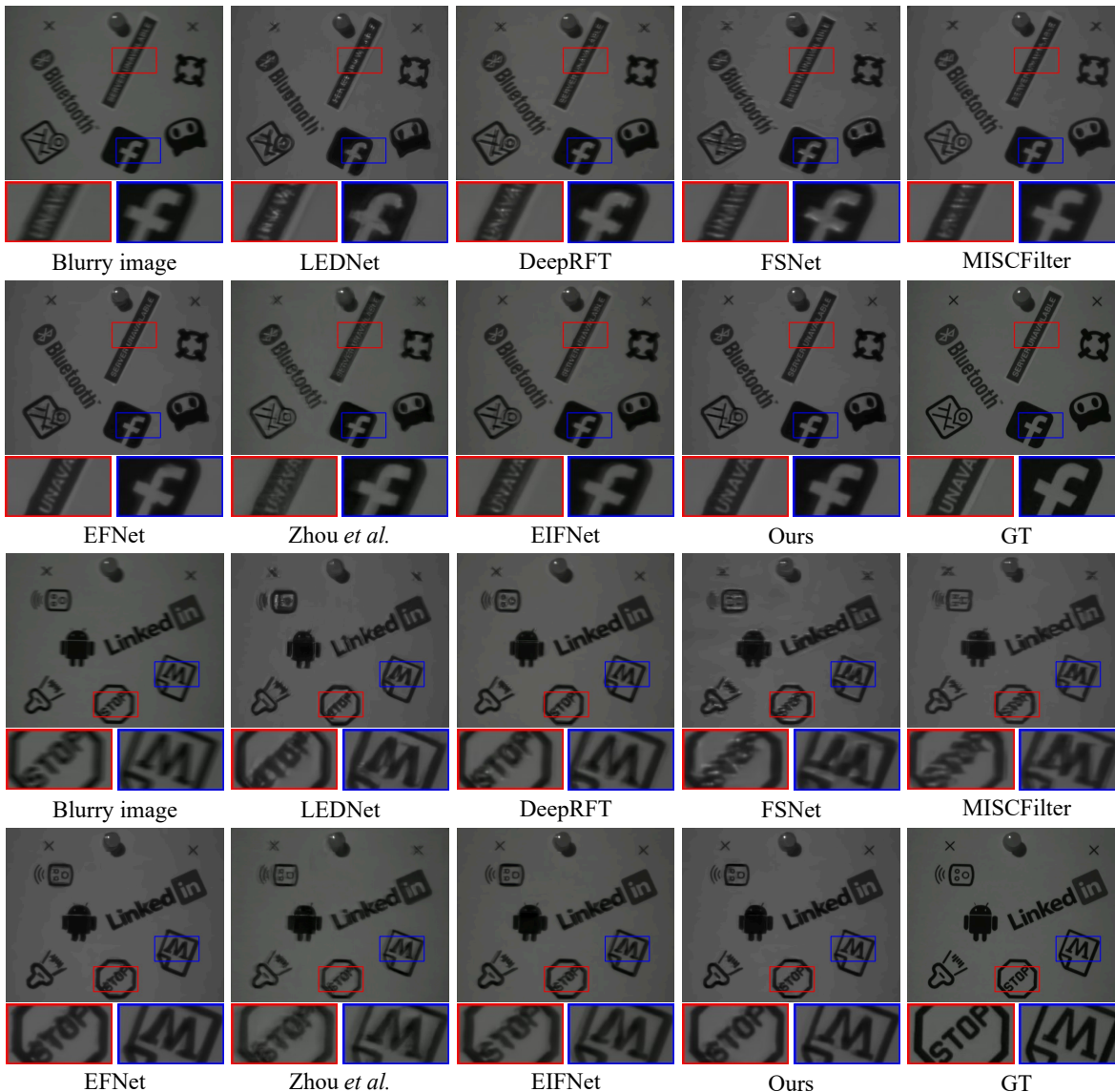


Fig. 15: Comparison results of our deblurring method with others on the CSDD dataset. The scene does not contain spectral inconsistency for both NIR and events.

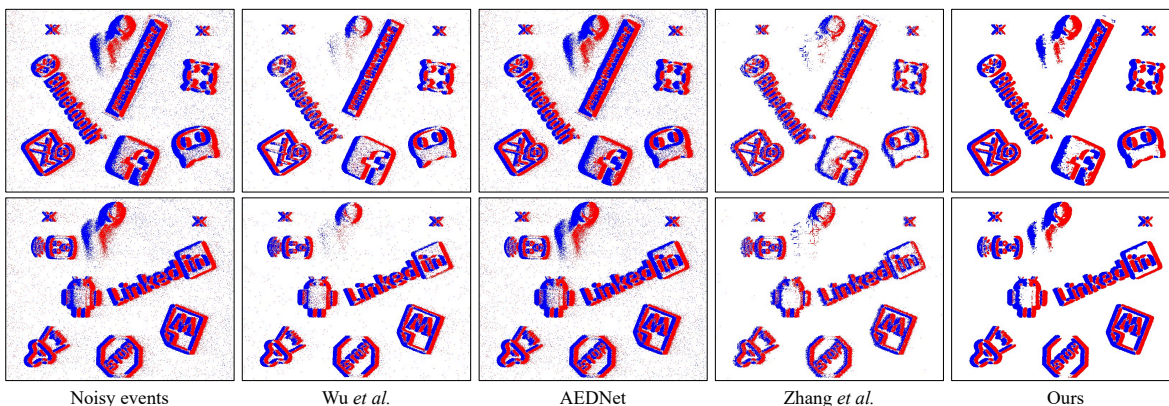


Fig. 16: Comparison results of our denoising method with others on the CSDD dataset. The events come from the same scene as the NIR in Fig. 15.

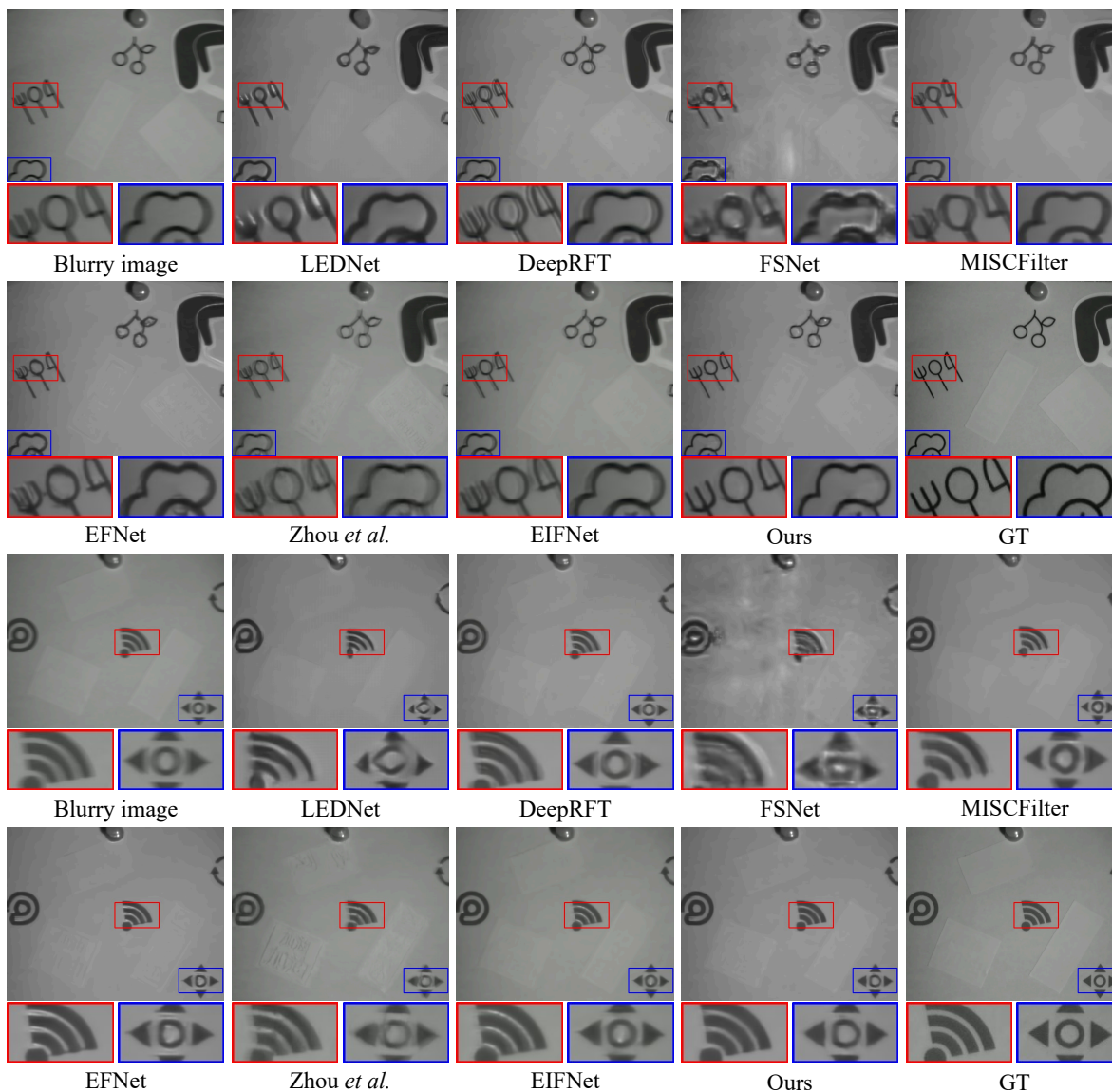


Fig. 17: Comparison results of our deblurring method with others on the CSDD dataset. The scene contains spectral inconsistency for both NIR and events.

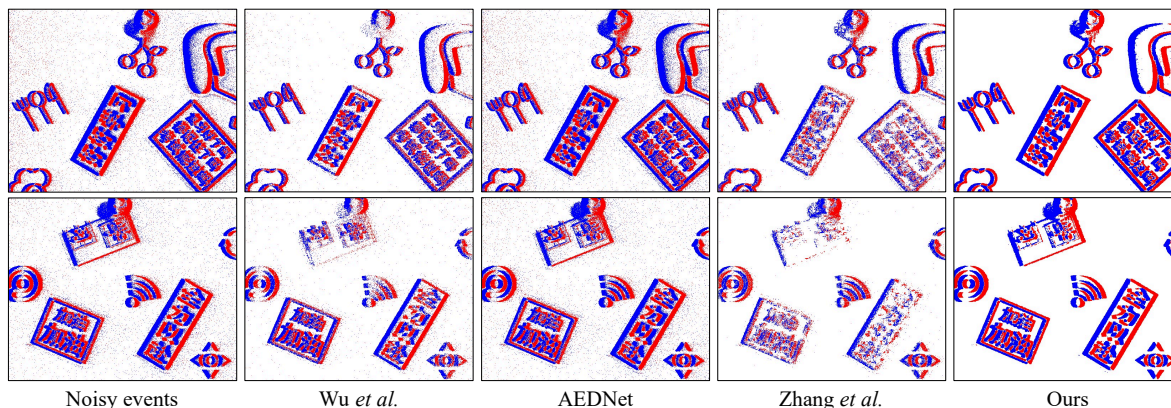


Fig. 18: Comparison results of our denoising method with others on the CSDD dataset. The events come from the same scene as the NIR in Fig. 17.

REFERENCES

- [1] C. Li, C. Guo, L. Han, J. Jiang, M.-M. Cheng, J. Gu, and C. C. Loy, “Low-light image and video enhancement using deep learning: A survey,” *IEEE Transactions on Pattern Analysis and Machine Intelligence*, vol. 44, no. 12, pp. 9396–9416, 2021.
- [2] J. Liu, D. Xu, W. Yang, M. Fan, and H. Huang, “Benchmarking low-light image enhancement and beyond,” *International Journal of Computer Vision*, vol. 129, pp. 1153–1184, 2021.
- [3] M. Niu, Z. Zhong, and Y. Zheng, “Nir-assisted video enhancement via unpaired 24-hour data,” in *Proceedings of the IEEE/CVF International Conference on Computer Vision*, pp. 10778–10788, 2023.
- [4] M. Geng, L. Zhu, L. Wang, W. Zhang, R. Xiong, and Y. Tian, “Event-based visible and infrared fusion via multi-task collaboration,” in *Proceedings of the IEEE/CVF Conference on Computer Vision and Pattern Recognition*, pp. 26929–26939, 2024.
- [5] Z. Li, H.-M. Hu, W. Zhang, S. Pu, and B. Li, “Spectrum characteristics preserved visible and near-infrared image fusion algorithm,” *IEEE Transactions on Multimedia*, vol. 23, pp. 306–319, 2020.
- [6] R. Xu, Z. Zhang, R. Wu, and W. Zuo, “Nir-assisted image denoising: A selective fusion approach and a real-world benchmark dataset,” *arXiv preprint arXiv:2404.08514*, 2024.
- [7] G. Gallego, T. Delbrück, G. Orchard, C. Bartolozzi, B. Taba, A. Censi, S. Leutenegger, A. J. Davison, J. Conradt, K. Daniilidis, and D. Scaramuzza, “Event-based vision: A survey,” *IEEE Transactions on Pattern Analysis and Machine Intelligence*, vol. 44, no. 1, pp. 154–180, 2022.
- [8] S. Zhu, C. Wang, H. Liu, P. Zhang, and E. Y. Lam, “Computational neuromorphic imaging: principles and applications,” in *Computational Optical Imaging and Artificial Intelligence in Biomedical Sciences*, vol. 12857, pp. 4–10, SPIE, 2024.
- [9] S. Jin, B. Yu, M. Jing, Y. Zhou, J. Liang, and R. Ji, “Dark-visionnet: Low-light imaging via rgb-nir fusion with deep inconsistency prior,” in *Proceedings of the AAAI Conference on Artificial Intelligence*, vol. 36, pp. 1104–1112, 2022.
- [10] Y. Cheng, R. Yang, Z. Zhang, J. Suo, and Q. Dai, “A mutually boosting dual sensor computational camera for high quality dark videography,” *Information Fusion*, vol. 93, pp. 429–440, 2023.
- [11] Q. Yan, X. Shen, L. Xu, S. Zhuo, X. Zhang, L. Shen, and J. Jia, “Cross-field joint image restoration via scale map,” in *Proceedings of the IEEE International Conference on Computer Vision*, pp. 1537–1544, 2013.
- [12] B. Yang, Z. Jiang, D. Pan, H. Yu, and W. Gui, “Detail-aware near infrared and visible fusion with multi-order hyper-laplacian priors,” *Information Fusion*, vol. 99, p. 101851, 2023.
- [13] N. Salamati, C. Fredembach, and S. Süsstrunk, “Material classification using color and nir images,” in *Color Imaging Conference*, pp. 216–222, 2009.
- [14] M. Brown and S. Süsstrunk, “Multi-spectral sift for scene category recognition,” in *CVPR 2011*, pp. 177–184, IEEE, 2011.
- [15] U. Schmidt, C. Rother, S. Nowozin, J. Jancsary, and S. Roth, “Discriminative non-blind deblurring,” in *Proceedings of the IEEE Conference on Computer Vision and Pattern Recognition*, pp. 604–611, 2013.
- [16] L. Xu, X. Tao, and J. Jia, “Inverse kernels for fast spatial deconvolution,” in *Computer Vision—ECCV 2014*, pp. 33–48, Springer, 2014.
- [17] T. F. Chan and C.-K. Wong, “Total variation blind deconvolution,” *IEEE Transactions on Image Processing*, vol. 7, no. 3, pp. 370–375, 1998.
- [18] J. Dong, J. Pan, Z. Su, and M.-H. Yang, “Blind image deblurring with outlier handling,” in *Proceedings of the IEEE International Conference on Computer Vision*, pp. 2478–2486, 2017.
- [19] X. Tao, H. Gao, X. Shen, J. Wang, and J. Jia, “Scale-recurrent network for deep image deblurring,” in *Proceedings of the IEEE Conference on Computer Vision and Pattern Recognition*, pp. 8174–8182, 2018.
- [20] S. Zhou, C. Li, and C. Change Loy, “Lednet: Joint low-light enhancement and deblurring in the dark,” in *European Conference on Computer Vision*, pp. 573–589, Springer, 2022.
- [21] M. Ren, M. Delbracio, H. Talebi, G. Gerig, and P. Milanfar, “Multiscale structure guided diffusion for image deblurring,” in *Proceedings of the IEEE/CVF International Conference on Computer Vision*, pp. 10721–10733, 2023.
- [22] X. Mao, Y. Liu, F. Liu, Q. Li, W. Shen, and Y. Wang, “Intriguing findings of frequency selection for image deblurring,” in *Proceedings of the AAAI Conference on Artificial Intelligence*, vol. 37, pp. 1905–1913, 2023.
- [23] X. Gao, T. Qiu, X. Zhang, H. Bai, K. Liu, X. Huang, H. Wei, G. Zhang, and H. Liu, “Efficient multi-scale network with learnable discrete wavelet transform for blind motion deblurring,” in *Proceedings of the IEEE/CVF Conference on Computer Vision and Pattern Recognition*, pp. 2733–2742, 2024.
- [24] C. Liu, X. Wang, X. Xu, R. Tian, S. Li, X. Qian, and M.-H. Yang, “Motion-adaptive separable collaborative filters for blind motion deblurring,” in *Proceedings of the IEEE/CVF Conference on Computer Vision and Pattern Recognition*, pp. 25595–25605, 2024.
- [25] L. Pan, C. Scheerlinck, X. Yu, R. Hartley, M. Liu, and Y. Dai, “Bringing a blurry frame alive at high frame-rate with an event camera,” in *Proceedings of the IEEE/CVF Conference on Computer Vision and Pattern Recognition*, pp. 6820–6829, 2019.
- [26] F. Xu, L. Yu, B. Wang, W. Yang, G.-S. Xia, X. Jia, Z. Qiao, and J. Liu, “Motion deblurring with real events,” in *Proceedings of the IEEE/CVF International Conference on Computer Vision*, pp. 2583–2592, 2021.
- [27] L. Sun, C. Sakaridis, J. Liang, Q. Jiang, K. Yang, P. Sun, Y. Ye, K. Wang, and L. V. Gool, “Event-based fusion for motion deblurring with cross-modal attention,” in *European Conference on Computer Vision*, pp. 412–428,

- Springer, 2022.
- [28] C. Zhou, M. Teng, J. Han, J. Liang, C. Xu, G. Cao, and B. Shi, “Deblurring low-light images with events,” *International Journal of Computer Vision*, vol. 131, no. 5, pp. 1284–1298, 2023.
- [29] T. Nakabayashi, K. Hasegawa, M. Matsugu, and H. Saito, “Event-based blur kernel estimation for blind motion deblurring,” in *Proceedings of the IEEE/CVF Conference on Computer Vision and Pattern Recognition*, pp. 4120–4128, 2023.
- [30] W. Yang, J. Wu, L. Li, W. Dong, and G. Shi, “Event-based motion deblurring with modality-aware decomposition and recomposition,” in *Proceedings of the 31st ACM International Conference on Multimedia*, pp. 8327–8335, 2023.
- [31] C. Zhang, X. Zhang, M. Lin, C. Li, C. He, W. Yang, G.-S. Xia, and L. Yu, “Crosszoom: Simultaneous motion deblurring and event super-resolving,” *IEEE Transactions on Pattern Analysis and Machine Intelligence*, 2024.
- [32] Z. Sun, X. Fu, L. Huang, A. Liu, and Z.-J. Zha, “Motion aware event representation-driven image deblurring,” in *European Conference on Computer Vision*, pp. 418–435, Springer, 2025.
- [33] B. Chakravarthi, A. A. Verma, K. Daniilidis, C. Fermuller, and Y. Yang, “Recent event camera innovations: A survey,” *arXiv preprint arXiv:2408.13627*, 2024.
- [34] C. Gabriel, T. Monfort, C. G. Specht, and I. Izeddin, “Event-based vision sensor for fast and dense single-molecule localization microscopy,” *Nature Photonics*, vol. 17, no. 12, pp. 1105–1113, 2023.
- [35] T. Delbruck *et al.*, “Frame-free dynamic digital vision,” in *Proceedings of Intl. Symp. on Secure-Life Electronics, Advanced Electronics for Quality Life and Society*, vol. 1, pp. 21–26, Citeseer, 2008.
- [36] S. Guo and T. Delbruck, “Low cost and latency event camera background activity denoising,” *IEEE Transactions on Pattern Analysis and Machine Intelligence*, vol. 45, no. 1, pp. 785–795, 2023.
- [37] Y. Feng, H. Lv, H. Liu, Y. Zhang, Y. Xiao, and C. Han, “Event density based denoising method for dynamic vision sensor,” *Applied Sciences*, vol. 10, no. 6, 2020.
- [38] P. Zhang, Z. Ge, L. Song, and E. Y. Lam, “Neuromorphic imaging with density-based spatiotemporal denoising,” *IEEE Transactions on Computational Imaging*, vol. 9, pp. 530–541, 2023.
- [39] A. Khodamoradi and R. Kastner, “O (n)-space spatiotemporal filter for reducing noise in neuromorphic vision sensors,” *IEEE Transactions on Emerging Topics in Computing*, vol. 9, no. 1, pp. 15–23, 2021.
- [40] R. Baldwin, M. Almatrafi, V. Asari, and K. Hirakawa, “Event probability mask (epm) and event denoising convolutional neural network (edncnn) for neuromorphic cameras,” in *Proceedings of the IEEE/CVF Conference on Computer Vision and Pattern Recognition*, pp. 1701–1710, 2020.
- [41] P. Duan, Z. W. Wang, X. Zhou, Y. Ma, and B. Shi, “Eventzoom: Learning to denoise and super resolve neuromorphic events,” in *Proceedings of the IEEE/CVF Conference on Computer Vision and Pattern Recognition*, pp. 12824–12833, 2021.
- [42] H. Fang, J. Wu, L. Li, J. Hou, W. Dong, and G. Shi, “Aednet: Asynchronous event denoising with spatial-temporal correlation among irregular data,” in *Proceedings of the 30th ACM International Conference on Multimedia*, pp. 1427–1435, 2022.
- [43] Y. Duan, “Led: A large-scale real-world paired dataset for event camera denoising,” in *Proceedings of the IEEE/CVF Conference on Computer Vision and Pattern Recognition*, pp. 25637–25647, 2024.
- [44] A. G. Howard, “Mobilenets: Efficient convolutional neural networks for mobile vision applications,” *arXiv preprint arXiv:1704.04861*, 2017.
- [45] Z. Jiang, Y. Zhang, D. Zou, J. Ren, J. Lv, and Y. Liu, “Learning event-based motion deblurring,” in *Proceedings of the IEEE/CVF Conference on Computer Vision and Pattern Recognition*, pp. 3320–3329, 2020.
- [46] P. Zhuang, J. Wu, F. Porikli, and C. Li, “Underwater image enhancement with hyper-laplacian reflectance priors,” *IEEE Transactions on Image Processing*, vol. 31, pp. 5442–5455, 2022.
- [47] A. Vaswani, N. Shazeer, N. Parmar, J. Uszkoreit, L. Jones, A. N. Gomez, Ł. Kaiser, and I. Polosukhin, “Attention is all you need,” *Advances in Neural Information Processing Systems*, 2017.
- [48] H. Rebecq, D. Gehrig, and D. Scaramuzza, “ESIM: an open event camera simulator,” in *Conference on Robot Learning*, pp. 969–982, 2018.
- [49] D. P. Kingma and J. Ba, “Adam: A method for stochastic optimization,” *arXiv preprint arXiv:1412.6980*, 2014.
- [50] P. Zhang, H. Liu, Z. Ge, C. Wang, and E. Y. Lam, “Neuromorphic imaging with joint image deblurring and event denoising,” *IEEE Transactions on Image Processing*, 2024.
- [51] Y. Cui, W. Ren, X. Cao, and A. Knoll, “Image restoration via frequency selection,” *IEEE Transactions on Pattern Analysis and Machine Intelligence*, 2023.
- [52] J. Wu, C. Ma, L. Li, W. Dong, and G. Shi, “Probabilistic undirected graph based denoising method for dynamic vision sensor,” *IEEE Transactions on Multimedia*, vol. 23, pp. 1148–1159, 2020.
- [53] G. Boracchi and A. Foi, “Modeling the performance of image restoration from motion blur,” *IEEE Transactions on Image Processing*, vol. 21, no. 8, pp. 3502–3517, 2012.
- [54] F. Lv, Y. Li, and F. Lu, “Attention guided low-light image enhancement with a large scale low-light simulation dataset,” *International Journal of Computer Vision*, vol. 129, no. 7, pp. 2175–2193, 2021.